Formation and Structure of Polyacrylamide–Silica Nanocomposites by Sol–Gel Process

JYONGSIK JANG, HWANSEOK PARK

Hyperstructured Organic Materials Research Center, School of Chemical Engineering, Seoul National University, San 56-1, Shinlimdong, Kwanakgu, Seoul 151-742, Korea

Received 24 August 2000; accepted 21 May 2001

ABSTRACT: The formation of nanocomposites by the sol–gel reaction of tetraethoxysilane (TEOS) in polyacrylamide (PAAm) is studied. The nanocomposites are prepared in aqueous solution. Fourier transform IR spectroscopy shows that substantial hydrogen bonding occurs in the nanocomposites. The fracture surfaces of the nanocomposites are observed by atomic force microscopy (AFM) as a function of the TEOS content. The AFM images reveal that the PAAm–silica nanocomposite exhibits particle–matrix morphology. It is also found that aggregate formation is more dominant than the particle growth with the TEOS contents. The solution of composite precursor is also applied to spin coating. Furthermore, during the calcination there is an observable change in the silica networks, and then a microinterconnected structure is generated.
 J Appl Polym Sci 83: 1817–1823, 2002

Key words: polyacrylamide–silica nanocomposites; atomic force microscopy; hydrogen bonding; silica gel; nanocomposite coating

INTRODUCTION

The sol–gel process is a chemical synthesis method initially used for the preparation of inorganic glasses.[1,2] Its mild reaction condition (i.e., low reaction temperature) allows the incorporation of an inorganic component into organic materials. Thus, the sol–gel process appears to be very convenient for the synthesis of organic–inorganic nanocomposite materials.

Organic–inorganic nanocomposite materials prepared by the sol–gel process were extensively studied in recent years.[3–9] The properties of a composite material depend not only on the properties of the individual components but also on the composite's phase morphology and interfacial properties. In the research for a novel nanocomposite, the morphology and phase separation should thus be regarded as critical factors. The nature of the interface between the organic and inorganic parts was used to classify hybrids into two different types. One class consists of two components, which are held by weak hydrogen bonds or van der Waals forces. In the other class the bonding between the organic and inorganic components is the covalent type.

Among several methods, *in situ* polymerization of an alkoxide within a polymer matrix is very simple and easily produces hybrid materials. This method is also interesting because it can be readily employed to improve commercial polymers. Polymers such as poly(methyl methacrylate),[10] poly(vinyl acetate),[11] poly(acrylic acid),[12] and poly(vinylpyrrolidone)[13] contain functional groups that can form hydrogen bonds and were successfully used to prepare hybrid materials.

Correspondence to: J. Jang (jsjang@plaza.snu.ac.kr).
Contract grant sponsor: Research Institute of Engineering Science.

Journal of Applied Polymer Science, Vol. 83, 1817–1823 (2002)

DOI 10.1002/app.10116

Acrylamide (AAm) polymers are an important class of materials because of their use in many industrial applications such as coats, flocculants, paper making, mining, and so forth.[14] Although the use of the AAm polymer has grown enormously, the nanocomposites based on polyacrylamide (PAAm) have not been investigated sufficiently. The organic polymer whose repeating units have *N*-alkyl or *N*,*N*-dialkylamide groups was studied previously.[15,16] The main focus of those studies was the porosity of inorganic materials. Organic polymers were used to generate the nanocomposites in organic solvents (i.e., methanol, THF, etc.).[15,16] However, the solubility of PAAm in a solvent is very restrictive. This limitation is an obstacle to the preparation of PAAm–silica nanocomposites.

In the present study PAAm–silica nanocomposite materials were prepared by the sol–gel method. The nanocomposites thus prepared were monolithic and thin film types. Fourier transform IR spectroscopy (FTIR), atomic force microscopy (AFM), and scanning electron microscopy (SEM) were utilized to prove the existence of an interaction between the two phases and to examine the morphological features of the hybrid materials. The surface of the thin film was also characterized by AFM.

In addition, it is necessary to consider both the morphology of the hybrid and the silica skeletal structure in order to understand the properties of hybrid materials. AFM has become a powerful instrument for the investigation of a variety of different material surfaces and interfaces.[17] It has some advantages in characterizing the surface of hybrid materials. Its images can be obtained without complicated and time-consuming sample preparation.

EXPERIMENTAL

Materials

The AAm (Merck, Darmstadt, Germany) was recrystallized from chloroform. The PAAm (M_w = 10,000 g/mol, 50 wt % aqueous solution, Aldrich, Milwaukee, WI) and tetraethoxysilane (TEOS, Merck) were used without further purification. The catalyst and solvent used were 0.1*M* HCl and distilled water, respectively.

Preparation of Hybrid Materials

PAAm–silica hybrid materials were prepared by the following process. The aqueous solution of PAAm was diluted with distilled water to 25 wt %. A mixture of TEOS, 0.1*M* HCl, and water was stirred vigorously to produce a homogeneous and transparent solution. Then the two solutions were mixed and stirred for 3 h. The compositions of the hybrid materials are shown in Table I. PAAm is soluble in water over the entire range of concentrations. As previously mentioned, common organic liquids including methanol, ethanol, and THF are nonsolvents for PAAm. Thus, the high water contents are necessary to prevent precipitation of PAAm in the precursor solution. The solution was placed in a polyethylene bottle and allowed to undergo gelation and drying at room temperature. After about 3 weeks, transparent and colorless hybrid materials were obtained as monoliths. Also, the precursor solution was spin coated at 2000 rpm on a glass substrate for 20 s. The coated film was then cured in air at 60°C for 5 h and 120°C for 3 h.

Table I Compositions of Samples

Sample	TEOS (wt %)[a]	PAAm (g)	TEOS (g)	0.1*M* HCl (g)	H_2O (g)
P33	33	2	1	1	10
P50	50	2	2	1	10
P67	67	1	2	1	8
P80	80	0.5	2	1	8
Sol–gel silica	100	—	2	1	8
M67	67	1 (AAm)	2	1	10

[a] Feed ratio.

Measurement

FTIR spectra were obtained in transmission mode between 400 and 4000 cm^{-1} using a Bomem MB100 with 4 cm^{-1} resolution. Samples were measured in the form of KBr pellets. AFM images were taken with a Digital Instruments Nanoscope IIIa atomic force microscope in the tapping mode with TESP nanoprobe tips. SEM measurement was conducted with a JSM 840-A.

RESULTS AND DISCUSSION

FTIR Analysis: Formation and Interaction of Nanocomposites

All the samples were transparent and monolithic glasses, regardless of the TEOS contents. This

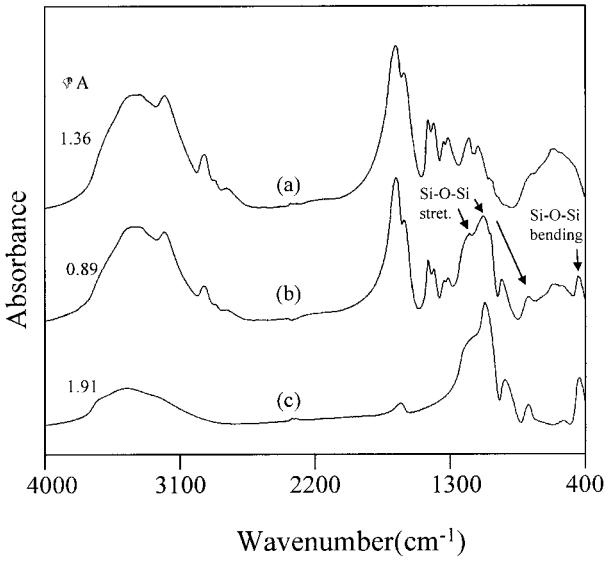

Figure 1 FTIR spectra of PAAm (spectrum a), P50 (spectrum b), and sol–gel silica (spectrum c).

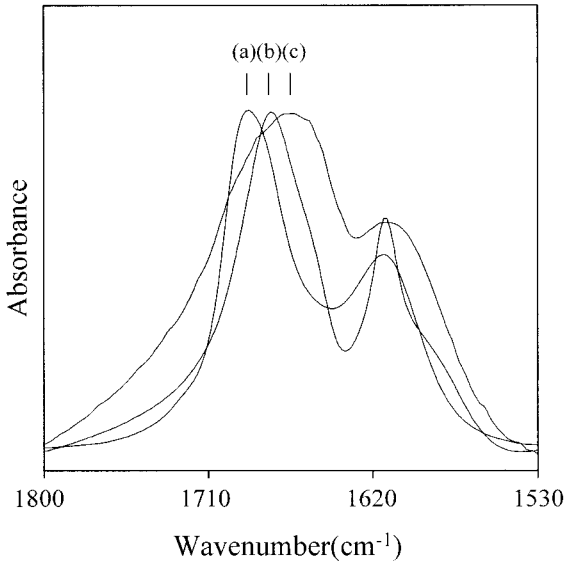

Figure 2 FTIR spectra of AAm in dioxane (spectrum a), M67 (spectrum b), and P67 (spectrum c).

indicates that strong interactions exist between PAAm and silica. IR spectroscopy has been one of the most utilized tools to study the structure of silica gel.[18,19] FTIR spectra of PAAm, P50, and a sol–gel silica sample are shown in Figure 1. The peaks at around 1220 and 1085 cm^{-1}, which are associated with the Si—O—Si asymmetric bond stretching vibration, were observed in P50 and sol–gel silica. The peaks at 796 and 460 cm^{-1} are related to a Si—O—Si symmetric bond stretching vibration and a Si—O—Si bending vibration, respectively. The presence of silanols on the silica networks is evidenced by the appearance of the hydroxyl peaks at 3100–3600 cm^{-1} and the Si—OH stretching peak at 950 cm^{-1}. These IR peaks confirm the formation of structural units of Si—O—Si in the samples.

In the PAAm–silica hybrid materials the presence of extensive hydrogen bonding between the silanols of the silica gel and the carbonyls of PAAm can be observed by using FTIR. The FTIR spectra of the AAm in dioxane, the AAm–silica hybrid, and the PAAm–silica hybrid are shown in Figure 2. In general, the shift of the carbonyl stretching peak to a low wavenumber is evidence of hydrogen bonding between the carbonyl groups of the polymer and the silanols of the silica gel.[15] Unfortunately, in the present samples it was difficult to directly show the low shift of the carbonyl peak of PAAm because PAAm is capable of extensive hydrogen bond formation between the PAAm chains themselves.[20] AAm monomer was employed to investigate the hydrogen bonding in the composite systems. As shown in Figure 2, the carbonyl peak of the AAm shifted from 1692 (AAm solution) to 1675 cm^{-1} (AAm–silica composite). The influence of the hydrogen bonding between AAm itself may be negligible because AAm was dispersed in the silica matrix. Thus, the low shift is the evidence of hydrogen bonding between the carbonyl group of AAm and the silanols of the silica gel (Fig. 3, structure I). Moreover, in the PAAm–silica hybrid, hydrogen bonding between the two phases could also be present. Additionally, inter- or intramolecular hydrogen

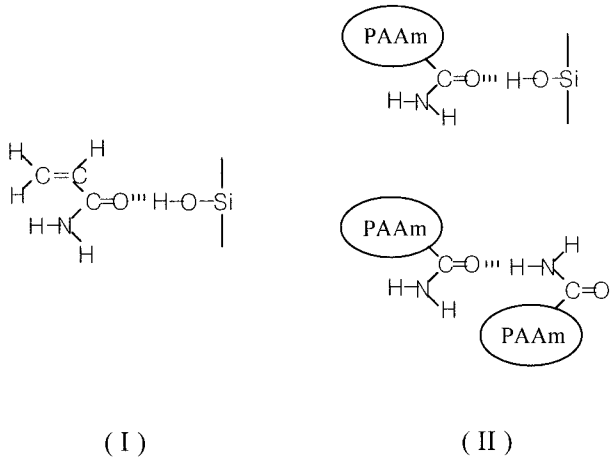

Figure 3 The tentative modes of hydrogen bonding in the monomer (structure I) and polymer (structure II).

bonds should be formed between the amide groups of the PAAm (Fig. 3, structure II). The shift of the carbonyl peak from 1675 to 1667 cm^{-1} (PAAm–silica composite) results from these interactions. However, it was not easy to distinguish the hydrogen bonding between PAAm and silanols from those of PAAm in an exact manner. We suggest the tentative hydrogen bonding modes (Fig. 3) from the FTIR results.

AFM Study: Morphological Properties of Nanocomposites

Succeeding steps in the polymerization from monomer to large particles and gels or powders in aqueous solution were schematically represented by Iler.[21] Brinker et al.[22] studied the polymerization of TEOS under acidic and basic conditions. Their results indicated that small, stable particles are produced under low pH conditions. Also, within the acid catalyst, gels prepared with relatively low water concentration exhibit extremely fine microstructure features and do not appear to be particulate. In contrast, gels appear to have a particulate structure at high water contents. The morphologies of P33 and the sol–gel silica gel observed by AFM are illustrated in Figure 4. The fracture surfaces were prepared immediately prior to scanning. P33 exhibits a smooth, random, and small grain size of about 16 nm. The sol–gel silica has similar trends except for the grain size. In P33 the mean roughness is 11.2 Å, and in the sol–gel silica it is 20.7 Å. Although P33 and sol–gel silica have different particle sizes, their roughness value is similar. The silica particles were well dispersed without aggregation and particle growth in the PAAm matrix. This may be due to hydrogen bonding, which can reduce macroscopic phase separation and stabilize the silica particles in the PAAm matrix and the concentration of TEOS. However, in spite of the acidic condition, sol–gel silica particle growth continues to form a larger size than P33. This is may be due to the high water contents.

Figure 5 shows the AFM top views of the fracture surfaces of the hybrid materials. As the TEOS contents increase, the silica particles tend to form aggregates. Mean roughness values as a function of the TEOS contents are presented in Figure 6. The mean roughness is the mean value of the surface relative to the center plane. The results show that the roughness values of the nanocomposite materials were affected by the TEOS contents. The AFM image of the sample at a low TEOS

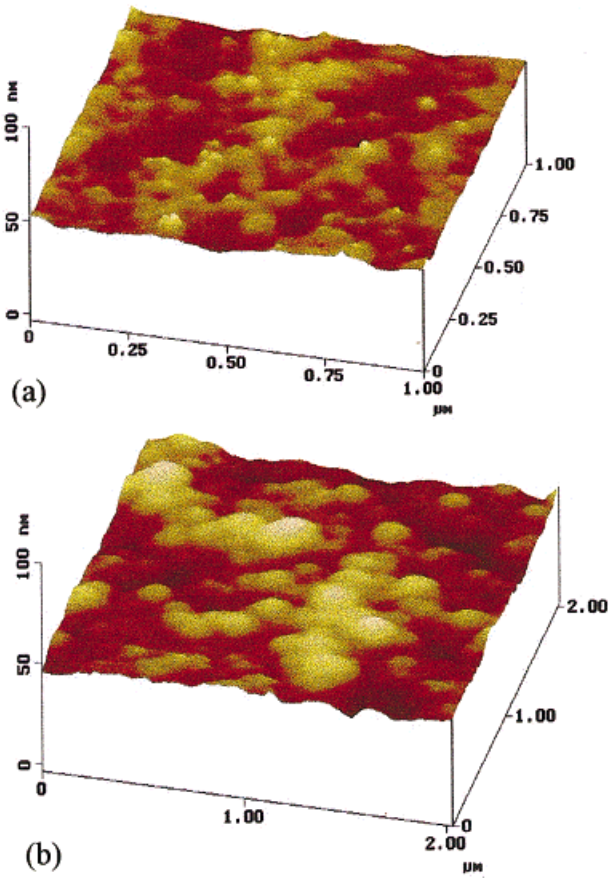

Figure 4 AFM topographic views of the fracture surfaces of (a) P33 and (b) sol–gel silica.

content (P33) is very smooth while those at higher TEOS contents show relatively greater roughness values and development of random aggregates.

Figure 7 illustrates AFM images of a glass substrate and spin-coated P50. The mean roughness of the glass substrate and coated P50 are 2.41 and 2.96 Å, respectively. The roughness of P50 is very similar to that of pure glass substrate, but the coated film has no defect on the surface. Compared with the morphology of the monolithic sample, there was no particulate properties in the thin film. These results suggest that the domain size of the silica segment in the thin film is very small, and the particle growth was restricted in the thin film system due to the geometrical limitation.

SEM Analysis: Silica Network after Calcination

Considering the applications, the control of the silica gel network is very important. Figure 8 shows the SEM micrographs of the nanocomposites before and after heat treatment at 800°C for

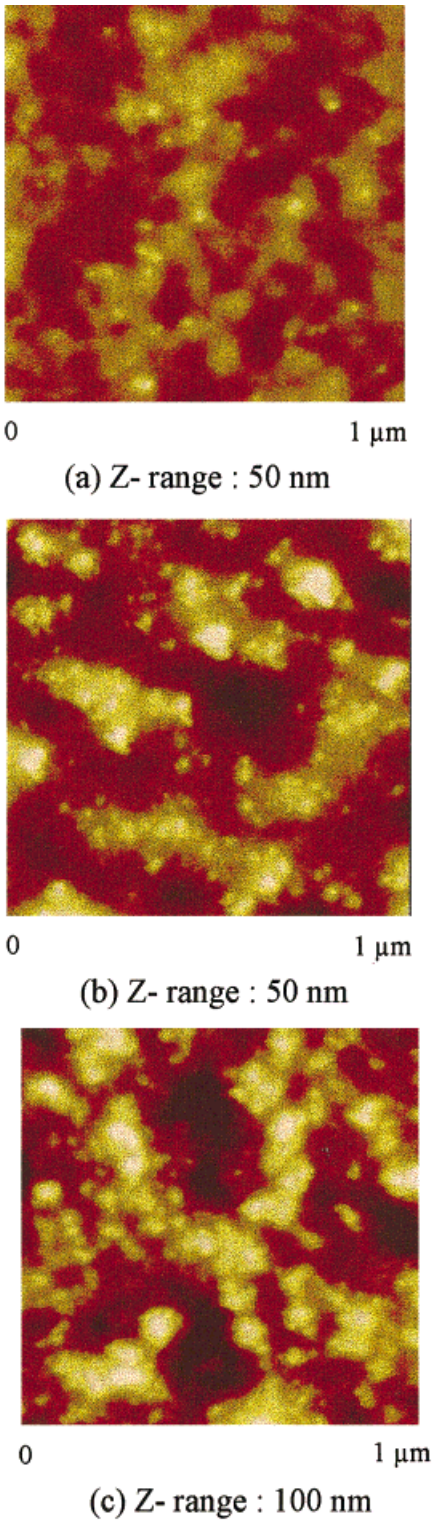

Figure 5 AFM top views of the fracture surfaces of (a) P33, (b) P67, and (c) P80 (1 × 1 m).

5 h. The SEM micrographs clearly show that the interconnected gel morphology was formed during calcination and its scale was micro. With an

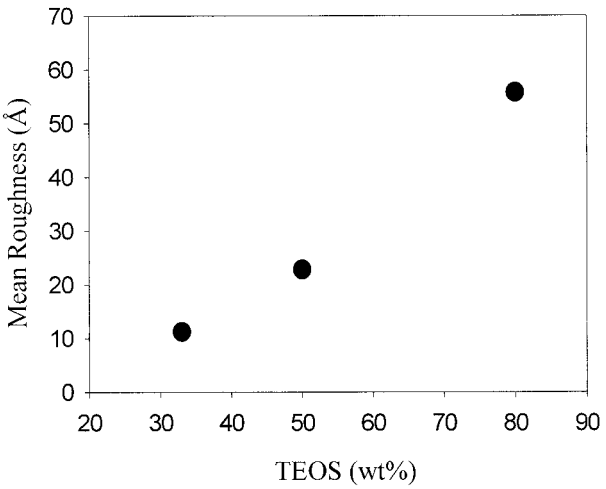

Figure 6 The effect of the TEOS contents on the mean roughness of the samples.

increase of TEOS contents, the width of the interconnected silica skeleton increases.

For the silica gels, removal of organic polymer is expected to collapse the particle–matrix mor-

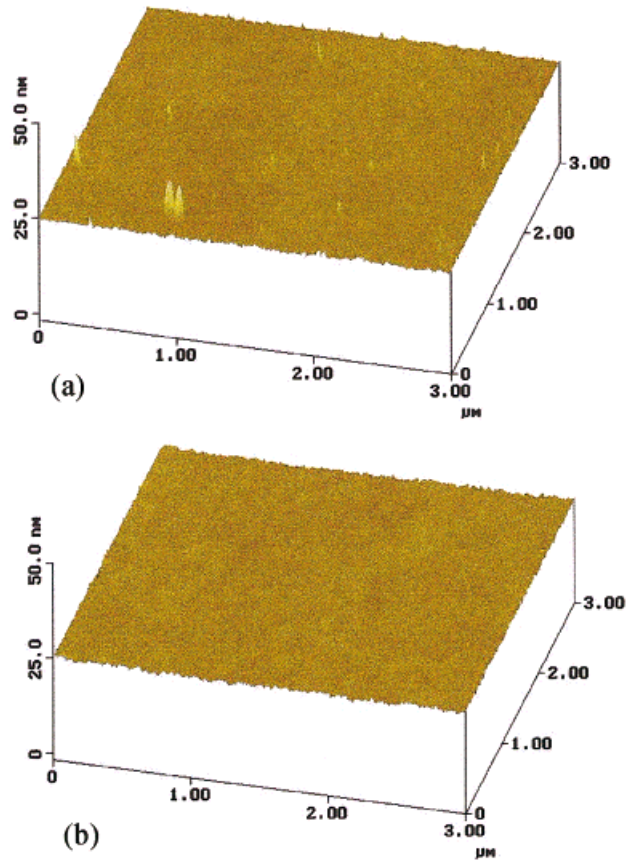

Figure 7 AFM topographic views of (a) the glass substrate and (b) spin-coated P50.

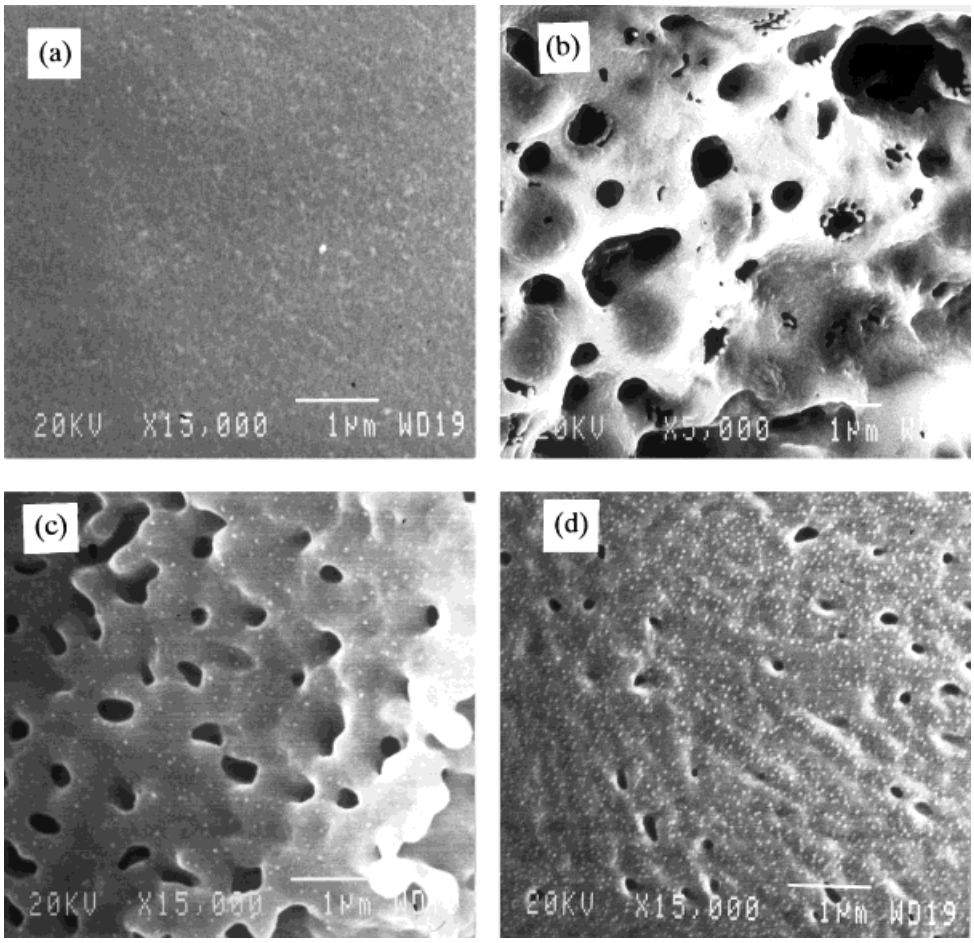

Figure 8 SEM micrographs of (a) P50, (b) thermally treated P33, (c) thermally treated P50, and (d) thermally treated P80 (800°C for 5 h).

phology, gradually resulting in additional cross-linking as unreacted hydroxyl and alkoxy groups come in contact. Thermal treatment may abruptly induce the change of the silica network.

Nakanishi and Soga used light scattering to study the phase separation of the composites.[12,23] Their results showed that silica gels with micrometer-range interconnected pores were prepared by the sol–gel process and the interconnected morphology was formed when the transitional structures of spinodal decomposition were frozen-in by the sol–gel transition of the inorganic components.[12,23]

CONCLUSION

Transparent PAAm–silica hybrid materials with hydrogen bonds were successfully prepared by the sol–gel process. The development of the observed morphology of the hybrid materials can be discussed in terms of the particle–matrix morphology. At low TEOS concentrations, the particles are well dispersed. These particles aggregate to form clusters with increasing TEOS contents. AFM studies of fracture surfaces showed that the hybrid materials appeared to form particulate properties, although under acidic conditions. This is due to the sufficient water concentrations. With an increase of TEOS contents, the roughness of the fracture surface and the aggregation of silica particles are increased. The nanocomposite film prepared by spin coating had an excellent flat surface without defects. Additionally, the silica gel cluster after calcination can be more compact and interconnected structures, and the interconnected silica gel network was microscale.

This research was carried out at and supported by the Research Institute of Engineering Science, and the authors gratefully acknowledge this support.

REFERENCES

1. Hench, L. L.; West, J. K. Chem Rev 1990, 90, 33.
2. Brinker, C. J.; Scherer, G. W. Sol–Gel Science: The Physics and Chemistry of Sol–Gel Processing; Academic: New York, 1990.
3. Novak, B. M. Adv Mater 1993, 5, 422.
4. Wen, J.; Wilkes, G. L. Chem Mater 1996, 8, 1667.
5. Sharp, K. G. Adv Mater 1998, 10, 1243.
6. Hajji, P.; David, L.; Gerard, J. F.; Pascault, J. P.; Vigier, G. J Polym Sci B Polym Phys 1999, 37, 3172.
7. Zhou, W.; Dong, J. H.; Qiu, K. Y.; Wei, Y. J Appl Polym Sci 1999, 73, 419.
8. Wojcik, A. B.; Klein, L. C. Appl Organomet Chem 1998, 11, 129.
9. Wu, K. H.; Chang, T. C.; Wang, Y. T.; Chiu, Y. S. J Polym Sci A Polym Chem 1999, 37, 2275.
10. Landry, C. J. T.; Coltrain, B. K.; Wesson, J. A.; Zumbulyadis, N.; Lippert, J. L. Polymer 1992, 33, 1496.
11. Landry, C. J. T.; Coltrain, B. K.; Landry, M. R.; Fitzgerald, J. J.; Long, V. K. Macromolecules 1993, 26, 3702.
12. Nakanishi, K.; Soga, N. J Non-Cryst Solids 1992, 139, 1.
13. Toki, M.; Chow, T. Y.; Ohnaka, T.; Samura, H.; Saegusa, T. Polym Bull 1992, 29, 653.
14. Kroschwitz, J. I. Encyclopedia of Polymer Science and Engineering, 2nd ed.; Wiley: New York, 1990.
15. Saegusa, T.; Chujo, Y. Makromol Chem Macromol Symp 1992, 64, 1.
16. Tamaki, R.; Naka, K.; Chujo, Y. Polym J 1998, 30, 60.
17. Wei, Y.; Jin, D.; Brennan, D. J.; Rivera, D. N.; Zhuang, Q.; DiNardo, N. J.; Qiu, K. Chem Mater 1998, 10, 769.
18. Bertduzza, A.; Fagnano, C.; Morelli, M. A.; Gotardi, V.; Guglielmi, M. J Non-Cryst Solids 1982, 48, 117.
19. Matos, M. C.; Ilharco, L. M.; Almeida, R. M. J Non-Cryst Solids 1992, 147–148, 232.
20. Colthup, N. B.; Daly, L. H.; Wiberley, S. E. Introduction to Infrared and Raman Spectroscopy; Academic: New York, 1975.
21. Iler, R. K. The Chemistry of Silica; Wiley: New York, 1979.
22. Brinker, C. J.; Keefer, K. D.; Schaefer, D. W.; Ashley, C. S. J Non-Cryst Solids 1982, 48, 47.
23. Nakanishi, K.; Soga, N. J Non-Cryst Solids 1992, 139, 14.